


# Characterization of chicken p53 transcriptional function via parallel genome-wide chromatin occupancy and gene expression analysis

Zhijie Chen,<sup>\*,†</sup> Lu Cui,<sup>\*</sup> Li Xu,<sup>\*</sup> Zheyi Liu,<sup>\*</sup> Yumeng Liang,<sup>\*</sup> Xuefeng Li,<sup>\*</sup> Yanhui Zhang,<sup>\*</sup> Yijing Li,<sup>†</sup> Shengwang Liu,<sup>\*</sup> and Hai Li <sup>\*,†,1</sup>

<sup>\*</sup>State Key Laboratory of Veterinary Biotechnology, National Poultry Laboratory Animal Resource Center, Harbin Veterinary Research Institute, the Chinese Academy of Agricultural Sciences, Harbin 150069, the People's Republic of China; <sup>†</sup>Heilongjiang Key Laboratory for Animal Disease Control and Pharmaceutical Development, College of Veterinary Medicine, Northeast Agricultural University, Harbin 150030, the People's Republic of China; and <sup>‡</sup>Department of Pathogenic Microbiology and Immunology, School of Basic Medical Sciences, Xi'an Jiaotong University, Xi'an 710061, the People's Republic of China

**ABSTRACT** The tumor suppressor p53, which acts primarily as a transcription factor, can regulate infections from various viruses in chickens. However, the underlying mechanisms of the antiviral functions of chicken p53 (**chp53**) remain unclear due to the lack of detailed information on its transcriptional regulation. Here, to gain comprehensive insights into chp53 transcriptional regulatory function in a global and unbiased manner, we determined the genome-wide chromatin occupancy of chp53 by chromatin immunoprecipitation, which was followed by sequencing and chp53-mediated gene expression profile by RNA sequencing using chemically immortalized leghorn male hepatoma (LMH) cells with ectopic expression of chp53 as the model. The

integrated parallel genome-wide chromatin occupancy and gene expression analysis characterized chp53 chromatin occupancy and identified 754 direct target genes of chp53. Furthermore, functional annotation and cross-species comparative biological analyses revealed the conserved key biological functions and DNA binding motifs of p53 between chickens and humans, which may be due to the consensus amino acid sequence and structure of p53 DNA-binding domains. The present study, to our knowledge, provides the first comprehensive characterization of the chp53 transcriptional regulatory network, and can possibly help to improve our understanding of p53 transcriptional regulatory mechanisms and their antiviral functions in chickens.

**Key words:** chicken, p53, chromatin immunoprecipitation sequencing, RNA sequencing

2022 Poultry Science 101:102164

<https://doi.org/10.1016/j.psj.2022.102164>

## INTRODUCTION

The tumor suppressor p53, is well known as 'the guardian of the genome' and is a transcription factor that controls a complex signal transduction network referred to as the p53 pathway (Vogelstein et al., 2000; Harris and Levine, 2005; Levine and Oren, 2009; Lawrence et al., 2014). Among the various biological processes of the p53 network, p53 has been shown to control many aspects of host immune responses, such as innate immunity, nitric oxide-induced apoptosis, and histocompatibility complex I expression (Albina et al., 1993; Messmer and Brune, 1996; Zhu et al., 1999; Thierry et

al., 2005; Xue et al., 2007; Lujambio et al., 2013; Schwitalla et al., 2013; Wang et al., 2013), all of which are important defence mechanisms of the host against viral infection. To date, the antiviral function of p53 has been confirmed in many viruses, such as vesicular stomatitis virus (Munoz-Fontela et al., 2005; Garijo et al., 2014), poliovirus (Pampin et al., 2006), hepatitis C virus (Dharel et al., 2008), and influenza A virus (Yan et al., 2015). For example, p53 plays an essential role in enhancing the type I IFN-mediated immune response against Influenza A virus (IAV) infection. Knockdown of p53 expression by RNAi enhanced IAV replication, which is associated with reduced expression of antiviral IFN-stimulated genes (ISGs), such as *IRF7*, *IRF9*, *ISG15*, *ISG20*, *GBP1*, *RIG-I*, and *OAS1*. In addition, pretreatment of p53-knockdown cells with IFN- $\alpha$  failed to inhibit IAV replication, showing impaired antiviral activity (Zhu et al., 2014). In chickens, Marek's disease virus must inhibit chicken p53 (**chp53**)-mediated

© 2022 The Authors. Published by Elsevier Inc. on behalf of Poultry Science Association Inc. This is an open access article under the CC BY-NC-ND license (<http://creativecommons.org/licenses/by-nc-nd/4.0/>).

Received January 12, 2022.

Accepted August 24, 2022.

<sup>1</sup>Corresponding author: [lihail\\_cau@163.com](mailto:lihail_cau@163.com)

transcriptional activity and apoptosis by interacting directly with chp53 via its Meq oncoprotein to replicate successfully (Deng et al., 2010). Efficient inhibition of the replication of J subgroup avian leukosis virus (ALV-J) (Zhang et al., 2021) and infectious bursal disease virus (Ouyang et al., 2017) by chp53 has been reported, which provides a direct link between chp53 function and the antiviral immune response in chickens. Our previous study also provided experimental evidence for the antiviral effect of chp53, which identified chp53 as the key determinant of avian infectious laryngotracheitis virus (ILTV) infection by suppressing ILTV replication in infected cells and protecting uninfected standby cells from ILTV-induced paracrine-regulated apoptosis, which reduces pathological damage and delays viral transmission (Li et al., 2018). However, the underlying molecular mechanisms by which chp53 represses infections of these avian viruses remain unclear.

At the molecular level, p53 acts primarily as a transcription factor, inducing a network of genes that contributes to its biological responses, including immune responses (Biegging and Attardi, 2012). Currently, p53 has been identified as a transcription factor for several important antiviral immune genes, such as genes encoding retinoic acid inducible gene I (Hsu et al., 2012), a ligand for NK-cell activating receptor NKG2D, Toll-like receptor 3, and NKG2D ligands ULBP1 and ULBP2 (Taura et al., 2008; Li et al., 2011; Textor et al., 2011; Shatz et al., 2012). The transcriptional regulatory networks of human and mouse p53 proteins and their target genes have been extensively studied (Li et al., 2012; Nikulenkov et al., 2012; Li et al., 2014; Jiang et al., 2015; Zhang et al., 2017), which demonstrates that the pleiotropic character of the p53 network makes it difficult to predict the consequence of p53 activation. Thus, discovery of the mechanisms governing p53-mediated biological outcomes is extremely important for application of p53-based therapies (Li et al., 2014). In chickens, the global characterization of the p53 transcriptional regulatory network is still lacking, which limits the in-depth illustration of the antiviral function of chp53.

In this study, to gain comprehensive insights into chicken p53 transcriptional regulatory function, we performed chromatin immunoprecipitation sequencing (ChIP-seq) and RNA sequencing (RNA-seq) to characterize p53 transcriptional responses in a global and unbiased manner. We characterized the important features of p53 chromatin occupancy and identified novel target genes.

## MATERIALS AND METHODS

### Cell Culture

The leghorn male hepatoma (LMH) cells (ATCC CRL-2117) were maintained in Dulbecco's modified Eagle's medium supplemented with 10% fetal bovine serum, 100 units/mL penicillin, 100  $\mu$ g/mL streptomycin, and 2 mM L-glutamine. Cell cultures were incubated at 37°C in 5% CO<sub>2</sub>. After the cells are recovered, they are passed to the fourth passage and then plated. For

RNA-seq and ChIP-seq, LMH cells were seeded in 100 mm dishes 12 h before transfection. Cells were harvested 24 h after transfection.

### Plasmids and Transfection

Chicken p53 cDNA was subcloned into the expression vectors p3xFLAG-CMV-7.1 to generate the recombinant plasmid Flag-chp53. These 2 plasmids were kindly provided by Zhiyong Ma and Yafeng Qiu (Shanghai Veterinary Research Institute, Chinese Academy of Agricultural Science, Shanghai, China). The LMH cells were plated onto tissue culture plates 12 h before transfection. Transfection was performed using the Turbofect transfection reagent (R0531, Thermo Scientific, Rockford, IL) according to the manufacturer's instructions. The transfection dose of both plasmids was 1  $\mu$ g/1.0  $\times$  10<sup>6</sup> cells.

### Flow Cytometry and Immunofluorescence

Fluorescence-activated cell sorting analyses were conducted using a BD FACScan cell sorter and CellQuest software version 4.0.2 (Becton Dickinson-Pharmingen, San Diego, CA). Cell death was assayed by examining cells in the sub-G1 phase of the cell cycle with propidium iodide-staining of permeabilized cells, as described previously (Li et al., 2011). For immunofluorescence staining, the samples were washed with PBS and fixed with 4% paraformaldehyde for 10 min. After quenching excess aldehyde, the samples were permeabilized with 0.1% Triton X-100. Nonspecific antibody binding was blocked with 2% bovine serum albumin for 1 h, and then the samples were incubated with a mouse anti-DYKDDDDK antibody (flag epitope tag, 1  $\mu$ g/mL; A00187, GenScript Corporation, Piscataway, NJ) against overexpressed chicken p53 or a mouse IgG2b isotype control antibody (1  $\mu$ g/mL; 53484, Cell Signaling Technology, Boston, MA), followed by a secondary FITC-conjugated goat anti-mouse antibody (1:64 dilution; F9006, Sigma-Aldrich, St. Louis, MO). All cell nuclei were stained with DAPI (2  $\mu$ g/mL; C1002, Beyotime Biotech, Jiangsu, China). Fluorescent signals were detected with an EVOS FL fluorescence microscope (AMG, Bothell, WA).

### Chromatin Immunoprecipitation Assays

Chromatin immunoprecipitation (ChIP) experiments were conducted as previously described (Wang et al., 2021) with some minor modifications. LMH cells were fixed in 1% formaldehyde for 10 min and then with 0.125 M glycine. DNA was sheared using a sonicator (6 mm; Cole Parmer, Chicago, IL) to an optimal DNA fragment size of 200 to 500 bp. Samples were kept ice cold throughout the sonication. Thirty cycles (30 s pulses/30 s rest) were set. Sonication amplitude was 30%. Each ChIP experiment was performed with sheared chromatin samples from LMH cells (5  $\times$  10<sup>6</sup> cells) using 5  $\mu$ g of one of the following antibodies: anti-flag or isotype control IgG2b. Protein A/G PLUS-agarose beads were

used for pull-down according to the manufacturer's instructions (sc-2003, Santa Cruz Biotechnology, Santa Cruz, CA). The immunoprecipitated DNA was purified using a QIAquick PCR Purification Kit (28106, QIAGEN, Valencia, CA). Chromatin immunoprecipitation followed by quantitative PCR (**ChIP-qPCR**) was performed using Luna Universal qPCR Master Mix (M3003L, NEB, Ipswich, MA) following the manufacturer's protocol with a Bio-Rad CFX96 instrument. The primer sequences are shown in [Table 1](#). All samples were measured in triplicate.

## RNA Sequencing and ChIP Sequencing

Genome-wide gene expression profiling and genome-wide chromatin occupancy of LMH cells was performed via RNA or DNA deep sequencing by Annoroad Gene Technology Co., Ltd. (Beijing, China), according to the manufacturer's instructions. Four biological replicates were performed for both ChIP-seq and RNA-seq experiments. For RNA-seq, RNA was isolated from cells using RNeasy Plus mini kit (74314, QIAGEN, Hilden, Germany) according to the manufacturer's instructions. For ChIP-seq, 10 ng ChIP DNA was prepared for HiSeq 2500 sequencing with TruSeq ChIP Sample Prep Kit (IP-202-1012, Illumina, San Diego, CA) following manufacturer instructions. Libraries for RNA-Seq were prepared with the TruSeq RNA Sample Prep Kits v2 (Illumina) following manufacturer instructions starting from the RNA fragmentation step. For sequencing, paired-end reads were obtained with the length of 150 bp. RNA-seq and ChIP-seq raw data were uploaded to the National Center for Biotechnology Information database under the accession number GSE193188 and GSE200405. Related statistics of all sequenced libraries (RNA-seq and ChIP-seq) have been added as supplementary data (Supplementary Table S3).

## RNA-seq Data Analysis

RNA sequencing (**RNA-seq**) data was analyzed with the Galaxy web-based tool ([Blankenberg et al., 2010](#)). Gene ontology and pathway analysis was performed with DAVID (gene enrichment analysis using the EASE score with a modified Fisher's exact test  $P$  value of  $< 0.05$  as the threshold ([Huang et al., 2009](#)).

## ChIP-seq Data Analysis

Chromatin immunoprecipitation sequencing (**ChIP-seq**) data analysis was performed with a web-based tool, Galaxy ([Blankenberg et al., 2010](#)), and R (<http://www.r-project.org/>). Venn diagrams were plotted with TBtools ([Chen et al., 2020](#)). The annotation and visualization of the ChIP peaks were performed using the ChIPseeker package ([Yu et al., 2015](#)). For de novo motif discovery analysis, we used the MEME program ([Bailey et al., 2015](#)). As input data, we used sequences at a distance  $\pm 50$  bp from the position of the peak maximum height.

**Table 1.** Primer sequences for ChIP-qPCR.

Gene	Primer direction <sup>a</sup>	Sequence (5' to 3')
<i>CDKN1A</i>	F	GCTGGGCTCAGACCTTCCCT
	R	AGCTCAGCAAGCAGCAGGAACAA
<i>MDM2</i>	F	TTTCGGAAGTGCTGTTGTTGCTG
	R	TCTGTAAGGCTGCTTTCCCAT
<i>DNMBP</i>	F	AACCCAGTGCAGAAGTTAGTGGA
	R	TCTGGAAACTAAGCACAAACCC
<i>CKAP5</i>	F	CATGCCCAGATGAACCAGA
	R	CGTTGCATAAATAGTGGCAAT
<i>FGFR1</i>	F	GCGGATAACACCAAGCCGAACC
	R	CGCCCCAACCAAGGCTCTACCAG
<i>HDDC2</i>	F	TATGGCTTCCCCTGTGGTC
	R	TGGTACAAGGTCAATGGCACT
<i>DMTN</i>	F	TCTCGCTTTGGGGCAGCTA
	R	TGCATGACCAGCGACCCGAAAC
<i>LIMK1</i>	F	CCCGTGGCCGACGATGCTG
	R	AGAGGACACGAGCACCC
<i>AHI1</i>	F	CAGCCTGTGTGCTTTGTCT
	R	CTCCCAAGCTTAAAGCA
<i>JMJD1C</i>	F	CCTCGGGCTGACATCACT
	R	AAAAGTACCAAACGCGCACT
<i>SLITRK4</i>	F	CCTAGCCACAAAGAACGAGG
	R	ATGGAACAAAACCGCTGTGA
<i>IQGAP2</i>	F	CCCCTCTTCTCTCCGGCCTC
	R	ACAGCGGCCAGAAAACCTGTC
<i>TUBGCP6</i>	F	CCAAGAAGGCAAACGGCCTC
	R	TACCACGGCTGAGTACAGA
<i>RCOR1</i>	F	TGACCCTCGGCCTTTCTCTCGG
	R	CCGGCAGCCTCCCGCAAAGC
<i>FAM46B</i>	F	TTGCAGACACAGCTGGGATCCAC
	R	GTGCTCAGCTGCGCTCCCT
<i>POU2F3</i>	F	GGTCCCCTTTCATCCATCCCT
	R	CAAGCTCTGCTGCGCCTG
<i>ABTB2</i>	F	CCGCAGCCCGCACAAATCCC
	R	CCCGCTTTCTCTTCGGTCCC
<i>BCAN</i>	F	CCACACAGCAGGGACCAT
	R	CGCACGCATCCATCCCTT
<i>CLASP2</i>	F	ACTGCCTCGTCTCGGAACCAA
	R	CCTGTCCACGTACCCGTCCT
<i>HDAC7</i>	F	CTTCCCAGGCCCATTTGTTGTG
	R	GTTCCACCTCCCGATGCTG
<i>INHBE</i>	F	CCCCTGCCCCTTTTACCCCTC
	R	AACGACCCCTATGGACACCT
<i>NUDT9</i>	F	ACCGCAGCCGTGACCAATCAGA
	R	CCGCTCCTGCCATTGGTGT
<i>DPP8</i>	F	CCGTGCTCAGCTGTGTGCTTCA
	R	CGCACAGCCCTCTCGTCCAG
<i>PIGK</i>	F	CCGCTTCTTCACTTTGCC
	R	CACTGCTGTACCAAACCCCAT
<i>SEH1L</i>	F	CAAAAAGTGGCATTTCAGTGACC
	R	ATACAGCCTTGTCTACGTT
<i>TNFRSF11A</i>	F	CTGTCTCGACGCTCCCGGAA
	R	TCCAACCGCTGCCACTCCGTGA
<i>FAM210A</i>	F	CCGCCGCTGTGTGACACC
	R	GAAGCACCCAGCAGCTCT
<i>NOL4</i>	F	GCAATGTTTCGCTGTCTCTC
	R	GTCCAACCTTTCTCTCGCAGT
<i>NDUFV2</i>	F	CCACAGCCGAGGTCCGCCAA
	R	CCCAGCCCTCTCCTTGAAGCC
<i>SNX27</i>	F	ACTACGTTTCCCCTCAGCCCGTG
	R	CTTACCCTCCTCGTCCGCCAT
<i>IGFBP3</i>	F	GGCCGTAACCTTAAGCCGAT
	R	ATGAATTACCAGCGGCACCAC
<i>MTF2</i>	F	CCCGAGTGGACCGTTCCCC
	R	CGCCTATTGTTCCCGGCACCC
<i>HSPD1</i>	F	CCACCCGGAAGTGAAGTCACT
	R	CGCCAAGCAGCAGTCAACC
<i>SLC2A11L1</i>	F	TAAGCCGTTTGAATCTCTCGT
	R	TGTTGCTGAAATTCGTTCT
<i>EYA1</i>	F	TGAACACTGGATAACCGCGTA
	R	TTGCTGCTCTCCCTCCGA
<i>LAMA1</i>	F	AGCCTAACTCTGCTCACACAACC
	R	AGCCTGCTCCATTCTAGCCAA
<i>P3H2</i>	F	CGTTGCTCCCTCCTTCGC

(continued)

**Table 1** (Continued)

Gene	Primer direction <sup>a</sup>	Sequence (5' to 3')
<i>PAX2</i>	R	CCGTATCCCAGTCCGGCTCC
	F	GGTTCTCCCAAAGCAAGCACCC
<i>FGD4</i>	R	CCTTCCCCGTAGATGGAACAGC
	F	GCTCCGAGTCCGTTTCCAGACC
<i>AGRN</i>	R	AGCCAGAACTTCACGCAACTCCC
	F	GCCATTAACCTGCCGTGAGCC
<i>HDAC9</i>	R	CCCCTGTAAGAAAGCCCGGAGA
	F	ATGCAGGCTCCAATCACCC
<i>PARM1</i>	R	GGCAGTGACAACTCATTTCATT
	F	CTCCGAGGCTTCTCACGGTCT
<i>BAIAP2L1</i>	R	ACCTGCTGGCATCGGCACCAC
	F	CCAAGTTTTGCACACCCGAG
<i>HNF1A</i>	R	TTTTGTCCCCAGTGTGACCC
	F	ATGTAAACAGATAGCCAAGGGT
<i>TBC1D32</i>	R	GTAACACGCCCGACTGTCA
	F	CCCTTTACGGGAGACCACGAC
<i>FBXO32</i>	R	CTCCCTTCGCTCGCCACCA
	F	CGCCGCCATGCCGTTCTCTCG
	R	AACCGCCGCTCTTCTCATCG

<sup>a</sup>F, forward; R, reverse.

The transcription factors (TFs) of the putative chp53 direct target genes were predicated using oPOSSUM v 3.0 (Ho Sui et al., 2005) based on the DNA sequences in the interval of  $\pm 100$  bp of the ChIP-seq peaks we identified. The parameters were as follows: conservation cut-off = 40%; matrix score threshold = 85%; results sorted by Fisher score; amount of upstream/downstream = 5000/5000. Protein interaction information was acquired using the STRING database (Szklarczyk et al., 2019). Cytoscape software (Shannon et al., 2003) was applied to visualize the protein interaction networks.

### RNA Extraction and Reverse Transcription-Quantitative PCR

Total RNA was extracted from cells using TRIzol reagent (Takara, Dalian, China). The quality and concentration of total RNA were measured using a microvolume spectrophotometer (Implen GmbH, Munich, Germany). A One-Step SYBR PrimeScript RT-PCR Kit (RR086A, Takara, Tokyo, Japan) was used for reverse transcription-quantitative PCR (RT-qPCR) according to the manufacturer's instructions. Primers sequences were designed using Oligo 7 software (version 7.6.0, Molecular Biology Insights, Inc., Colorado Springs, CO). The primer sequences are shown in Table 2. All samples were measured in triplicate. The relative quantification of target gene expression was calculated by  $2^{-\Delta\Delta C_t}$  method.

### Western Blot Analysis

Western blot was performed strictly according to previously described procedures (Wang et al., 2019). Briefly, cells were washed with ice-cold PBS and soluble proteins were extracted with cell lysis buffer (100 mM Tris-HCl [pH = 8], 150 mM NaCl, 1% NP-40, phosphatase and protease inhibitor cocktail tablets [S8820, Sigma-Aldrich])

**Table 2.** Primer sequences for RT-qPCR.

Gene	Primer direction <sup>a</sup>	Sequence (5' to 3')
<i>CDKN1A</i>	F	CCCCTAGACCACGAGCAGAT
	R	CGTCTCGGTCTCGAAGTTGA
<i>MDM2</i>	F	ATTCTCAGCCATCTACGTCA
	R	TGAGATGTCTGTTTTGCCAT
<i><math>\beta</math>-actin</i>	F	GTGGATCAGCAAGCAGGAGT
	R	ATAAAGCCATGCCAATCTCGT
<i>BLVRA</i>	F	ACATTTTACAGGCAGTGTCC
	R	GTCAATCAGCCAAGTCAGTCCG
<i>TP63</i>	F	AGCAAGTCTCTGACAGCACA
	R	TGACCCGCAAGTACAAGAGC
<i>PKP1</i>	F	CTCCAGCAACAAGCCCGAT
	R	CGTGCCACCATCTATCTCGT
<i>HOPX</i>	F	GCCTCATTGCAGCTGAGACC
	R	CAGCCCTTCAGACTTCTCTCC
<i>MAMDC2</i>	F	AAACATTCGCAATTTCCAGT
	R	GATTAGCTGAGCCACCTCC
<i>ASTN2</i>	F	ATGTCCCTGAAACCAGCCTCT
	R	AGTTCTGAGTGTCTCCCTCGT
<i>ACVR1C</i>	F	ATCGACATCCCGCAGAACC
	R	CCGTGCTATCTCCCAGTACACC
<i>GAS2L1</i>	F	CGTCTCCAACCTTCATCCGCTGGT
	R	TGGCCACCTCCAGCAAGCAG
<i>CA9</i>	F	TCCGAGCACACCGTTGACCAC
	R	AGCACTGCCAGCCATCCG
<i>FAIM</i>	F	GTATCCAAAAACAAGAGCCACT
	R	CTCCATATATTTCTTGAGGCTT
<i>NEDD9</i>	F	ACAACCTGGTCTTTGAATGTGCTC
	R	TTGCCACCATAACAAACCGAT
<i>LOC416263</i>	F	AGATGGCTACAACACAGCTGACA
	R	GCAACCTCCCAATGCTCCCAA
<i>CITED2</i>	F	ATGCTGCCGCCCAATGTCA
	R	GCGATCCAGCCCATTTTCGAT
<i>SLC2A11L1</i>	F	CTTATGCTTTTAATGGTGGCTT
	R	CAGGTAGACAAAAGATAGCCA
<i>EYA1</i>	F	TCCCCACCACAGATTTACCC
	R	CCTGTTGTAACCTGCGTCT
<i>LAMA1</i>	F	GGCAAAGTCCCAGCATTTCAGA
	R	AAAATCCAGTTTCCAGGTCGT
<i>P3H2</i>	F	AGCAAACGCAGCTCACACCT
	R	CCAACCCGTAATCCTCCTTGTC
<i>PAX2</i>	F	CTCCAAGCCCAAAGTAGCG
	R	CCGAATCTCCCAAGCCAAAC
<i>FGD4</i>	F	AGCAGCATCTGTCCAAAGTCC
	R	ACTGTTTACTGGCACACT
<i>AGRN</i>	F	ATGGCCTCACCTATGACAACCCG
	R	CCCCTGAGCCACATTCGTCC
<i>HDAC9</i>	F	CTGCCACCATACCTCACT
	R	TGGGAAATCATCCTTGGCATC
<i>PARM1</i>	F	CGAAGAAGGCAAAAGCACTCCC
	R	CCCGAAGACCAGCACTACCAC
<i>BAIAP2L1</i>	F	TAAAGAGGTACCAAACCGAAC
	R	CTCCATTTCTTATGCTCGT
<i>HNF1A</i>	F	TACACCTGGTACGTCCGCAAG
	R	AGGACCCCACTTAAAGCGAT
<i>TBC1D32</i>	F	TTTTATCTGGATCCGAGCTT
	R	AGCCATAAGGAATTAGCATC
<i>FBXO32</i>	F	ACAGCCTTAACTATGATGTTGC
	R	CAGTAACCATGGCGCTCT

<sup>a</sup>F, forward; R, reverse.

according to the manufacturer's protocol. The protein concentration of each sample was determined by a BCA Kit (P0012, Beyotime Biotech). An equal amount of protein was separated by SDS-PAGE and transferred onto a nitrocellulose membrane (Millipore, Billerica, MA). The membrane was then blocked with 5% non-fat milk for 2 h at room temperature and incubated with primary antibodies overnight at 4°C. Antibodies were obtained from GenScript Corporation (A00187) and Proteintech (1:3000 dilution;  $\beta$ -actin, 60008-1-Ig, Wuhan, China). Signals

were visualized using infrared imaging systems (Odyssey CLX, LiCor Biosciences, Lincoln, NE).

### p53 Amino Acid Sequence and Structure Analysis

The p53 amino acid sequences were aligned using MegAlign program (DNASTAR 7.1, DNASTAR Inc., Madison, WI). Next, Conserved Domain Database-search tool in NCBI (<https://www.ncbi.nlm.nih.gov/cdd/>) and MEME (Bailey et al., 2015) was used to predict the conserved domains of proteins. Finally, we use the online website Phyre2 (Kelley et al., 2015) to predict the three-dimensional structure of the protein.

### Statistical Analysis

The SPSS software package (SPSS for Windows version 13.0, SPSS Inc., Chicago, IL) was used for all statistical analyses. Data obtained from several experiments are reported as the mean  $\pm$  standard deviation (SD).

The significance of differences between 2 groups was determined with two-tailed unpaired Student's *t* test. For all analyses, a probability (*P*) value of  $< 0.05$  was considered statistically significant.

## RESULTS

### Genome-Wide Map of Chicken p53 Binding to Chromatin Upon Its Ectopic Overexpression

Due to the lack of an ideal monoclonal antibody for the ChIP of chicken p53 (chp53), the ectopic overexpression of chp53 was conducted in LMH cells which have been used as an in vitro model to study the viral-host interactions of ILTV in our previous studies (Li et al., 2016, 2018; Wang et al., 2019; Qiao et al., 2020; Wang et al., 2021). Chp53 was overexpressed in LMH cells by transfecting a Flag-chp53 plasmid (Deng et al., 2010). The efficiency of overexpression was determined by indirect immunofluorescence (Figure 1A) and flow

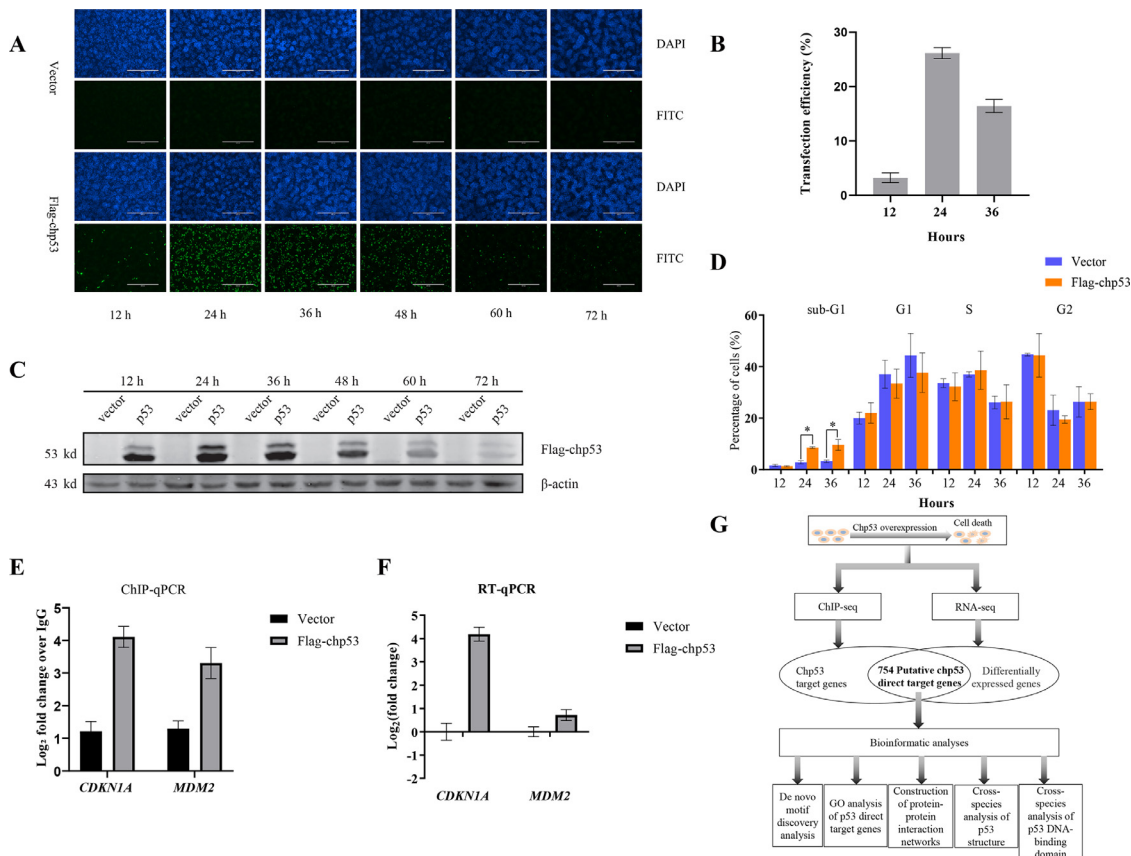


**Figure 1.** Experimental model and design. LMH cells were transiently transfected with Flag-chp53 or empty vector p3xFLAG-CMV-7.1(vector). (A and B) Indirect immunofluorescence microscopy and flow cytometry analyses of p53 overexpression using a mouse anti-flag antibody followed by a FITC-conjugated goat anti-mouse IgG secondary antibody (green) at 12 h, 24 h, 36 h, 48 h, 60 h, and 72 h or 12 h, 24 h, and 36 h post-transfection. Chromosomes were stained with DAPI (blue). Scale bars, 400  $\mu$ m. (C) The protein expression levels of chicken p53 (chp53) in LMH cells transiently transfected with the Flag-chp53 or vector plasmid were analyzed by Western blot using antibodies specifically against Flag (top) and  $\beta$ -actin (bottom).  $\beta$ -actin was used as a loading control. (D) LMH cells were transiently transfected with Flag-chp53 plasmid or negative control empty vector for 24 h. Cell-cycle profiles were determined by fluorescence-activated cell sorting of propidium iodide-stained cells. (E and F) LMH cells were transfected with a vector or Flag-chp53 plasmid and harvested at 24 h. (E) Chromatin immunoprecipitation sequencing (ChIP-seq) assays were performed with an anti-Flag antibody. IgG2b was used as a negative control. ChIP-qPCR analysis of the relative p53 occupancies in the promoters of *CDKN1A* and *MDM2* in LMH cells. (F) The mRNA levels of *CDKN1A* and *MDM2* were determined by RT-qPCR in LMH cells. (G) Illustration of the experimental workflow. Abbreviation: LMH, leghorn male hepatoma.

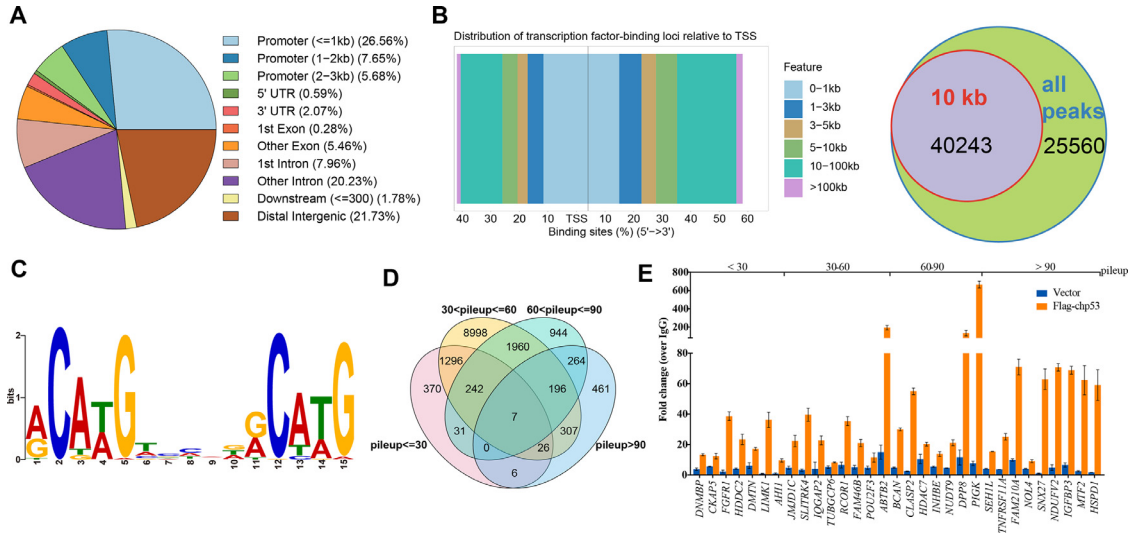


**Figure 2.** Genome-wide characterization of chp53 binding sites. For ChIP-seq data, thresholds of  $P < 0.01$ ,  $q < 0.01$ , and fold change  $> 2$  were applied. (A) Binding of chp53 is located in different parts of the gene. (B) Chp53 binding sites are located at varying distances from the TSS. A Venn diagram demonstrates the proportion of p53-bound fragments located within  $\pm 10$  kb of the TSS (40,243 out of 65,803). (C) The chp53 consensus binding motif was identified de novo by analyzing the sequences of 65,803 peaks using the MEME program. (D) Venn diagram showing the intersections of the genes bound by p53 (within 10 kb from TSS) from different pileup regions. (E) ChIP-qPCR was used to determine the relative p53 occupancies in the binding sites of 31 selected genes in LMH cells upon ectopic expression of chp53. ChIP-qPCR data are presented as the means  $\pm$  SDs ( $n = 3$ ). Abbreviation: LMH, leghorn male hepatoma.

cytometry (Figure 1B) analyses using an antibody targeting Flag, which revealed the highest transfection efficiency at 24 h after transfection. Furthermore, Western blot assays revealed ectopic chp53 expression starting 12 h after transfection, with the highest level of chp53 expression occurring at 24 h (Figure 1C). In this in vitro model, LMH cells were transiently transfected with Flag-chp53 plasmid or negative control empty vector for 24 h. Chp53 overexpression induced significant levels cell death but not cell cycle arrest, as assayed by fluorescence-activated cell sorting of propidium iodide-stained cells (Figure 1D).

*CDKN1A* and *MDM2* have been experimentally identified as the direct target genes of chicken p53 (Deng et al., 2010). The amount of overexpressed p53 bound to the transcription regulating regions of these two classic chp53 target genes were quantified by ChIP-qPCR in LMH cells upon ectopic expression of chp53. Input DNA was used as a positive control, and ChIP with an isotype IgG2b antibody was used to determine the level of non-specific binding of the antibody to DNA. Increased binding of overexpressed chp53 to the transcription-regulating regions of these 2 genes was observed upon ectopic expression of p53 by ChIP-qPCR (Figure 1E). The transcriptional activity of chp53 bound to these 2 genes was validated by the increased transcription levels of these 2 genes after chp53 overexpression as assayed by RT-qPCR (Figure 1F). These results demonstrate that in our in vitro model, overexpressed chp53 could successfully interact with its binding sites on chromatin with an activated transcriptional regulatory function. Using this model, ChIP-seq and RNA-seq were conducted to obtain the genome-wide chromatin occupancies of chp53 in LMH cells and related gene expression profiles (Figure 1G).

We performed ChIP-seq of chp53 in LMH cells upon chp53 overexpression. Thresholds of  $P < 0.01$ ,  $q < 0.01$ , and fold change  $> 2$  were applied, with 65,803 peaks corresponding to chp53-bound DNA fragments identified upon chp53 overexpression in LMH cells. The locations of chp53-bound DNA fragments around genes are summarized in Figure 2A. The promoter region accounted for 39.89%, 5' UTR accounted for 0.59%, 3' UTR accounted for 2.07%, exon region accounted for 5.74%, intron region accounted for 28.19%, immediate downstream region, which is the proximal intergenic region ( $\leq 300$  bp) accounted for 1.78%, and the distal intergenic region accounted for 21.73%. Although chp53 binding sites were located in varying parts of the genes, approximately 60% of chp53-bound fragments were located within  $\pm 10$  kb of the transcription start site (TSS; Figure 2B).

We generated a consensus p53-binding site based on p53-bound fragments by applying the de novo motif discovery algorithm, MEME, for the 65,803 peaks (E-value =  $2.1 \times 10^{-56}$ ; Figure 2C), which fits well with the original human p53 consensus site as well as the one refined later (Wei et al., 2006; Riley et al., 2008; Smeenk et al., 2008; Menendez et al., 2009). Figure 2D summarizes the amounts of p53-binding sites in different pileup (pileup height at peak summit) regions. As shown in the Venn diagram, approximately 28.69% of these p53-bound genes have multiple p53 binding sites.

For validation purposes, 31 putative chp53 binding sites were selected randomly from each pileup region and the occupancy of chp53 at each site in LMH cells upon ectopic expression of p53 was determined by ChIP-qPCR. As shown in Figure 2E, all these selected putative chp53 binding sites were successfully validated with no significant differences in validation rates among different pileup regions.

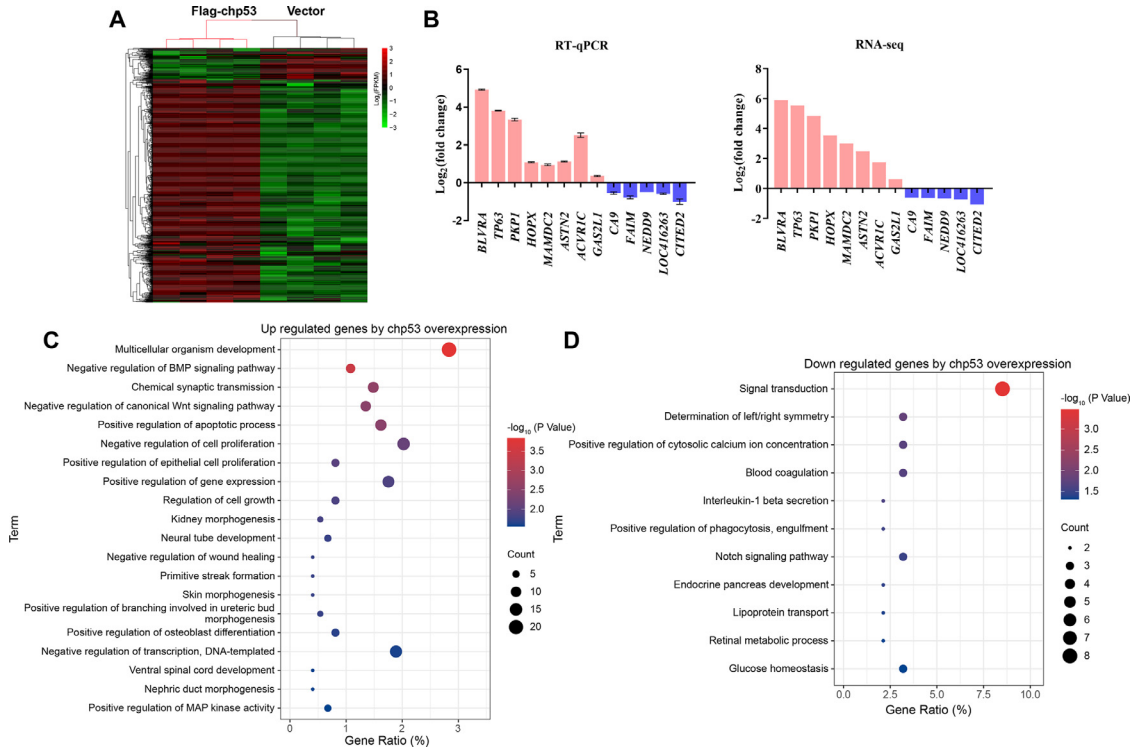


**Figure 3.** Genome-wide transcriptome analysis of LMH cells upon chp53 overexpression. (A) Hierarchical clustering analysis of 923 genes that were differentially expressed in LMH cells at  $P < 0.01$ ,  $q < 0.01$ , and fold change of  $> 1.5$ . Columns indicate arrays, and rows indicate genes. The values are normalized by row. Green indicates downregulation and red indicates upregulation. The color scale represents the  $\log_2$  expression levels (FPKM, fragments per kilobase of exon per million fragments mapped) of each gene. (B) The transcriptions of 13 genes selected to validate the RNA sequencing data were assayed by reverse transcription-quantitative PCR. Data are presented as the means  $\pm$  SDs ( $n = 3$ ). Gene ontology analysis was performed with DAVID ( $P < 0.05$ ) (C and D). (C) Biological processes of 809 upregulated genes by chp53 overexpression. (D) Biological processes of 114 downregulated genes by chp53 overexpression. Abbreviation: LMH, leghorn male hepatoma.

### Identification of Chicken p53 Target Genes

Next, we explored the effects of the ectopic expression of chp53 on the gene expression profiles in LMH cells via RNA-seq. Bioinformatics analysis identified 923 genes that were differentially expressed upon ectopic expression of chp53 based on the following criteria: 1)  $P$  value of  $< 0.01$ , 2)  $q$  value of  $< 0.01$ , and 3) fold change of  $> 1.5$ . Hierarchical clustering analysis using these differentially expressed genes (DEGs) indicated efficient clustering of biological replicates for each group of cells (Figure 3A). Compared with the control cells, 114 genes were downregulated and 809 were upregulated in LMH cells upon ectopic expression of p53 (Supplementary Table S1). For validation, the transcript levels of 13 genes randomly selected from the 923 DEGs were examined by RT-qPCR analysis. The directions of change determined by RT-qPCR detection and transcriptome sequencing analysis were generally identical (Figure 3B), suggesting a correspondence between these 2 methods in our study. Additional Gene Ontology analysis revealed that the upregulated DEGs were significantly enriched in biological processes such as regulation of the canonical Wnt signaling pathway, apoptosis, gene expression, and cell growth (Figure 3C). The downregulated DEGs were significantly enriched in biological processes such as signal transduction, cytosolic calcium ion concentration, and the Notch signaling pathway (Figure 3D).

Analysis of chp53 occupancy showed that chp53 bound to 40,243 sites corresponding to 15,108 genes (Figures 2D and 4A). Among these genes, the transcription of only 675 genes was induced (83.44% of upregulated DEGs) and 79 genes were repressed (69.30% of downregulated DEGs) upon ectopic expression of p53 (Figure 4A), suggesting that these 754 DEGs are putative direct chp53 target genes (Supplementary Table S2). Among these putative direct chp53 target genes, 8 induced and 5 repressed genes were selected randomly for validation. The binding of chp53 to these genes was confirmed by ChIP-qPCR and the transcriptional regulation of chp53 to these genes was validated by RT-qPCR in LMH cells upon ectopic chp53 expression (Figure 4B), suggesting that these 754 genes are bona fide chp53 target genes. A total of 169 genes that changed their expressions upon ectopic expression of chp53 were not bound by chp53 and most likely represent secondary effects of p53. The transcriptions of the majority of the genes bound by chp53 remained unaffected, suggesting that the binding of chp53 per se is not sufficient to regulate gene expression. Consistent with the finding that the majority of DEGs induced by ectopic chp53 expression were bound by chp53 (Figure 4A), further functional annotation of the putative chp53 target genes that were induced or repressed by chp53 showed similar results to those of induced or repressed DEGs (Figures 4C and D), indicating direct

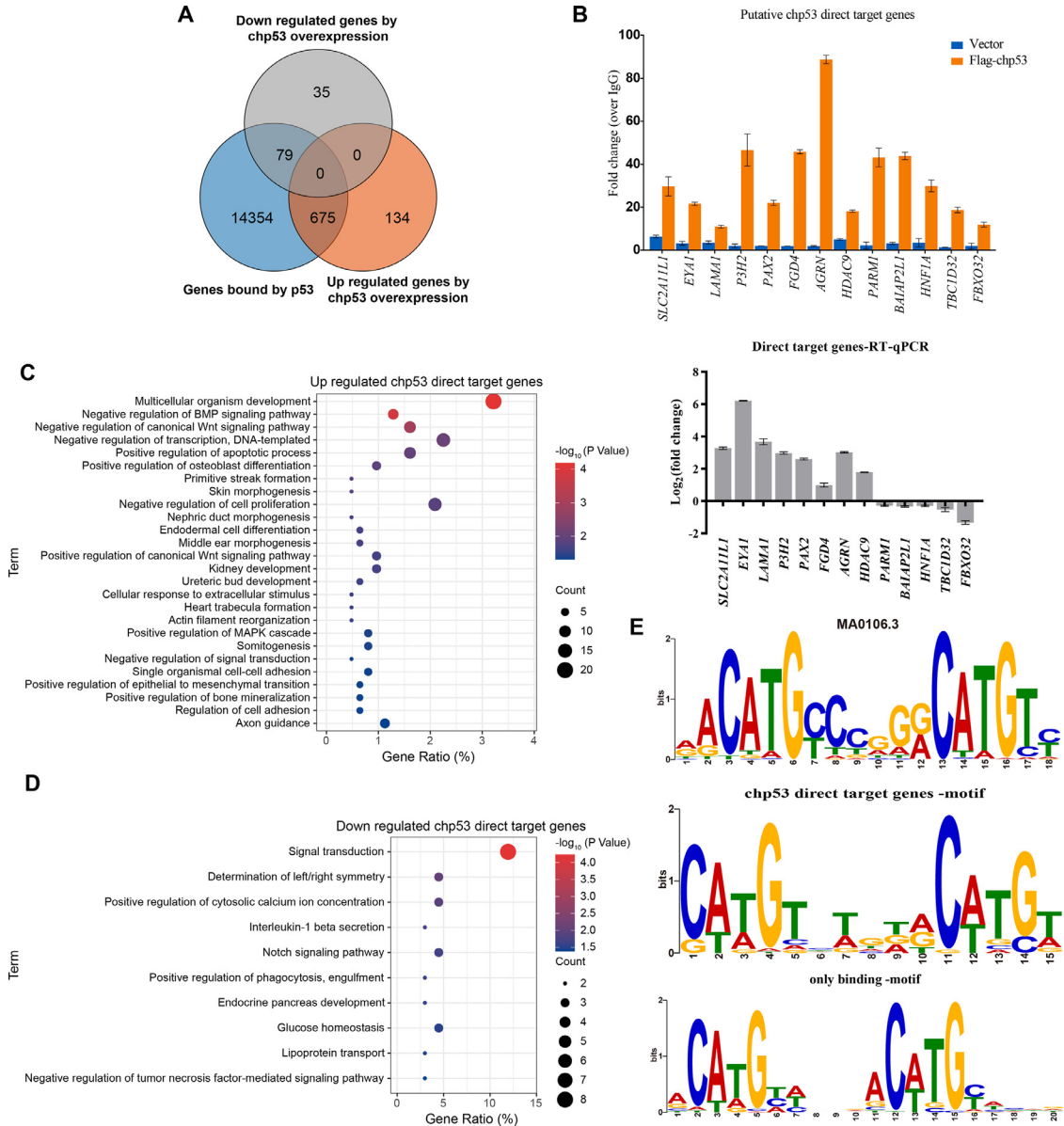


**Figure 4.** Identification of chp53 target genes in LMH cells upon chp53 overexpression. (A) Bioinformatic analysis of the genes bound by p53 within  $\pm 10$  kb of the TSS and differentially expressed upon ectopic expression of chp53 for 24 h revealed 754 putative chp53 direct target genes. (B) Validation of chromatin occupancies and mRNA expressions in a selected panel of newly identified p53 direct target genes. ChIP using the antibody Flag, followed by qPCR, was used to determine the relative p53 occupancies in the promoters of 13 selected genes in LMH cells upon ectopic expression of chp53 (upper panel). The mRNA levels of 13 selected genes were determined by RT-qPCR in LMH cells upon ectopic expression of p53 (bottom panel). Data are presented as the means  $\pm$  SDs ( $n = 3$ ). (C and D) Gene ontology analysis was performed with DAVID ( $P < 0.05$ ). (C) Biological process results from upregulation of putative chp53 direct target genes. (D) Biological process results from the downregulation of putative chp53 direct target genes. (E) The p53 consensus binding site was analyzed using the only-binding p53-bound fragments (14354-motif) or p53-bound fragments of chp53-target genes (675+79-motif), respectively, using the MEME algorithm. Abbreviation: LMH, leghorn male hepatoma.

transcriptional control of these biological processes by chp53. We generated two chp53-binding motifs based on the p53-bound fragments of the chp53-target genes we identified (754 genes; E-value =  $5.9 \times 10^{-8}$ ) and the only-binding p53-bound fragments (14,354 genes; E-value =  $4.2 \times 10^{-4}$ ), respectively, using the de novo discovery algorithm MEME (Bailey et al., 2015). Two identical motifs were obtained, both of which are highly similar to the classic human p53 consensus motif (Figure 4E), indicating high conservation of the p53 binding motif among species.

### Cross-Species Analysis of p53 Transcriptional Regulation Networks

To determine the central modulators of the molecular network in LMH cells upon ectopic expression of p53, we performed TFs prediction using oPOSSUM v 3.0 (Ho Sui et al., 2005) based on the DNA sequences in  $\pm 100$  bp intervals of the ChIP-seq peaks we identified. Twenty-nine TFs, including p53, were predicted to be the key regulators of the transcriptional shift induced by chp53 overexpression in LMH cells (Z score  $\geq 10$  and



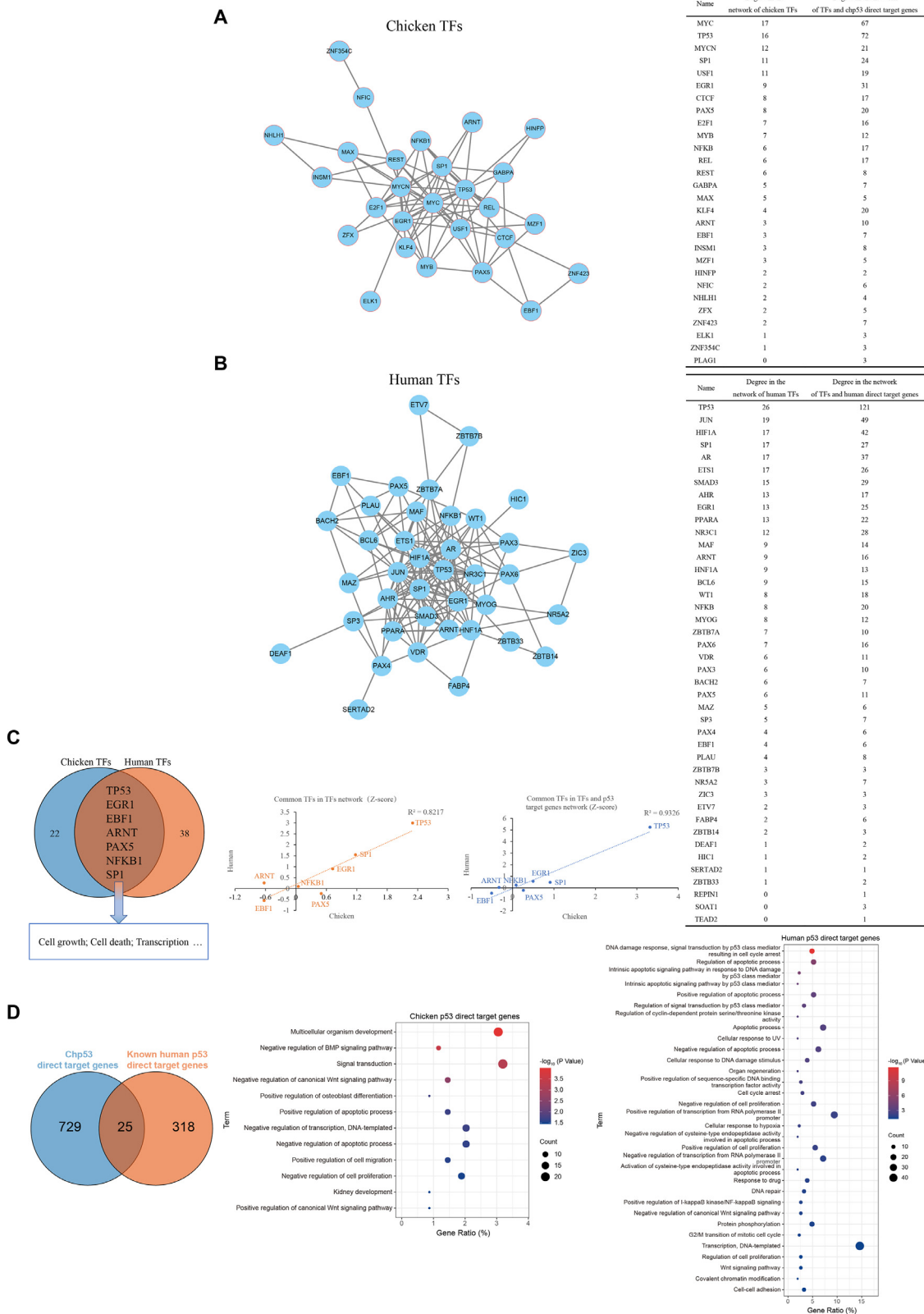


**Figure 5.** Construction of the chicken p53 regulatory network. (A and B) Analysis of the functional interactions among the transcription factors (TF) (left) or TF together with direct target genes (Supplementary Figures S1 and S2) reveals p53 as the most promising central modulator of the molecular events. The TF nodes were arranged in order of their functional connectivity to other proteins in the TF network (right). (A) TFs predicted by the p53-bound fragment sequences in chicken p53 direct target genes. (B) Human TFs were derived from a published human p53 dataset (Nikulenkov et al., 2012). (C) Venn diagram shows that seven of the human and chicken TFs are identical (left). The correlations analysis of the seven common TFs (middle and right). The Z score of chicken and human TFs in the TF network or TF together with p53 direct target gene network were calculated by normalizing the degree (middle and right). (D) Venn diagram showing the intersections of chicken p53 direct target genes and human p53 direct target genes (left). Gene ontology analysis of chicken p53 direct target genes (middle) and human p53 direct target genes (right) ( $P < 0.05$ , count  $> 5$ ).

Fisher score  $\geq 7$ ) and were submitted for protein interaction analysis using the STRING database (Szklarczyk et al., 2019). The protein-protein interaction networks of these TFs or these TFs together with the chp53 target genes we identified were visualized by Cytoscape program (Shannon et al., 2003), with the layout of group attributes determined according to the connectivity degrees of the nodes (Figure 5A and Supplementary Figure S1). A similar analysis of a published human p53 dataset was also conducted (Nikulenkov et al., 2012), and 45 TFs were predicted to be the key regulators of the transcription network of human p53 (Figure 5B and Supplementary Figure S2). As expected, both chp53 and human p53 were predicted to be some of the most central transcriptional regulators with high number of connections with other key TFs and their target genes in their own transcriptional networks. Among these TFs, only 6 were common between chickens and humans, except p53 itself (Figure 5C), which is consistent with the great difference in p53 target genes between the 2 species (Figure 5D). Similar findings were observed when comparing human and mouse data (Tonelli et al., 2017; Supplementary Figure S3).

However, many well-known p53-mediated biological processes related to cell proliferation, apoptosis, and transcription are commonly enriched by both chicken and human p53 target genes (Figure 5D). Consistently, among the 6 common TFs, SP1, EGR1, PAX5, and NFkB have been identified as the essential coregulators of p53 in these p53-mediated biological processes (Figure 5C; Liu et al., 2011; Zwang et al., 2012; Li et al., 2014; Huang et al., 2016), suggesting the conservation of p53 key functions between species.

To gain an in-depth understanding of the above findings, protein alignments of chicken, human, and mouse p53 proteins were performed using ClustalW (MegAlign, DNASTar 7.1.0) with their full amino acid sequences. The sequence distances indicated the divergence and percent identity values of each sequence pair in the current alignment. Divergence is calculated by comparing sequence pairs in relation to the phylogeny reconstructed by MegAlign. Percent identity compares sequences directly, without accounting for phylogenetic relationships (Figure 6A, lower left panel). These analyses revealed obvious differences in the sequences among chickens and the other species (Figure 6A, upper panel). In addition, a phylogenetic tree was constructed using the neighbor-joining method to view the evolutionary relationships predicted from the above multiple sequence alignments. The length of each pair of branches represents the distance between sequence pairs, while the units at the bottom of the tree indicate the number of substitution events. A dotted line on a phenogram indicates a negative branch length, a common result of averaging (Figure 6A, lower right panel). The results show that the evolutionary relationship between chicken and human or between chicken and mouse p53 proteins is distant. This finding was further proven by 3D in silico models generated using the amino acid sequences of p53 (e.g., chicken NP\_990595.1, human NP\_000537.3 and

mouse NP\_035770.2; Figure 6B). However, analysis of the conserved domains of p53 proteins from different species indicates the structural and functional conservation of p53 proteins from different species, suggesting that these p53 proteins from different species all perform regulation through similar signaling pathways (Figure 6C). Furthermore, prediction of the secondary structure suggests that these p53 proteins in different species can maintain relatively conservative and stable functional topological folding structures, which is consistent with the higher homology and domain conservation at the level of their primary structure (Figure 6D), indicating that p53 proteins from different species may have similar functions.

Thus, alignments of the amino acid sequences of the DNA binding domain of p53 proteins were also conducted using ClustalW, which revealed better identities and lower divergences among chicken p53 and p53 of other species compared with those of the full sequences of p53 proteins (Figure 7A). The phylogenetic tree analysis also indicated closer evolutionary relationships between the chicken and human or between chicken and mouse p53 DNA-binding domains. Meanwhile, the conserved motifs of the DNA binding domains of p53 proteins were further analyzed using MEME (Bailey et al., 2015) and 2 conserved motifs in p53 proteins were identified among species (Figure 7B), which further confirmed the conservation of the DNA binding domains of the p53 protein sequence. The 3D in silico models were generated using the amino acid sequences of these p53 DNA-binding domains (Figure 7C). The predictions of the secondary structures suggests that these p53 DNA-binding domains from different species can maintain highly conserved and stable functional topological folding structures, which is consistent with the higher homology and domain conservation at the level of their primary structures. This proves that p53 proteins from different species have similar DNA binding domains, leading to their identical DNA binding motifs and may have conserved transcriptional regulating functions (Figure 7D).

## DISCUSSION

The effects of p53 on viral infections have been demonstrated in chickens, including our previous studies, which identified chp53 as a key determinant of ILTV infection (Li et al., 2018). However, due to the lack of fundamental information on the chp53 transcription regulatory network, the underlying molecular mechanisms of the antiviral function of chp53 remain unclear. Here, to gain deeper insights into chicken p53 functions, we integrated ChIP-seq and RNA-seq analyses to describe the genome-wide binding and direct regulation of genes by chp53 in chickens using LMH cells with ectopic expression of chp53 as the model and identified 754 direct chp53 target genes. Additional functional analysis and comparative biological analysis among species revealed conserved key biological functions and DNA



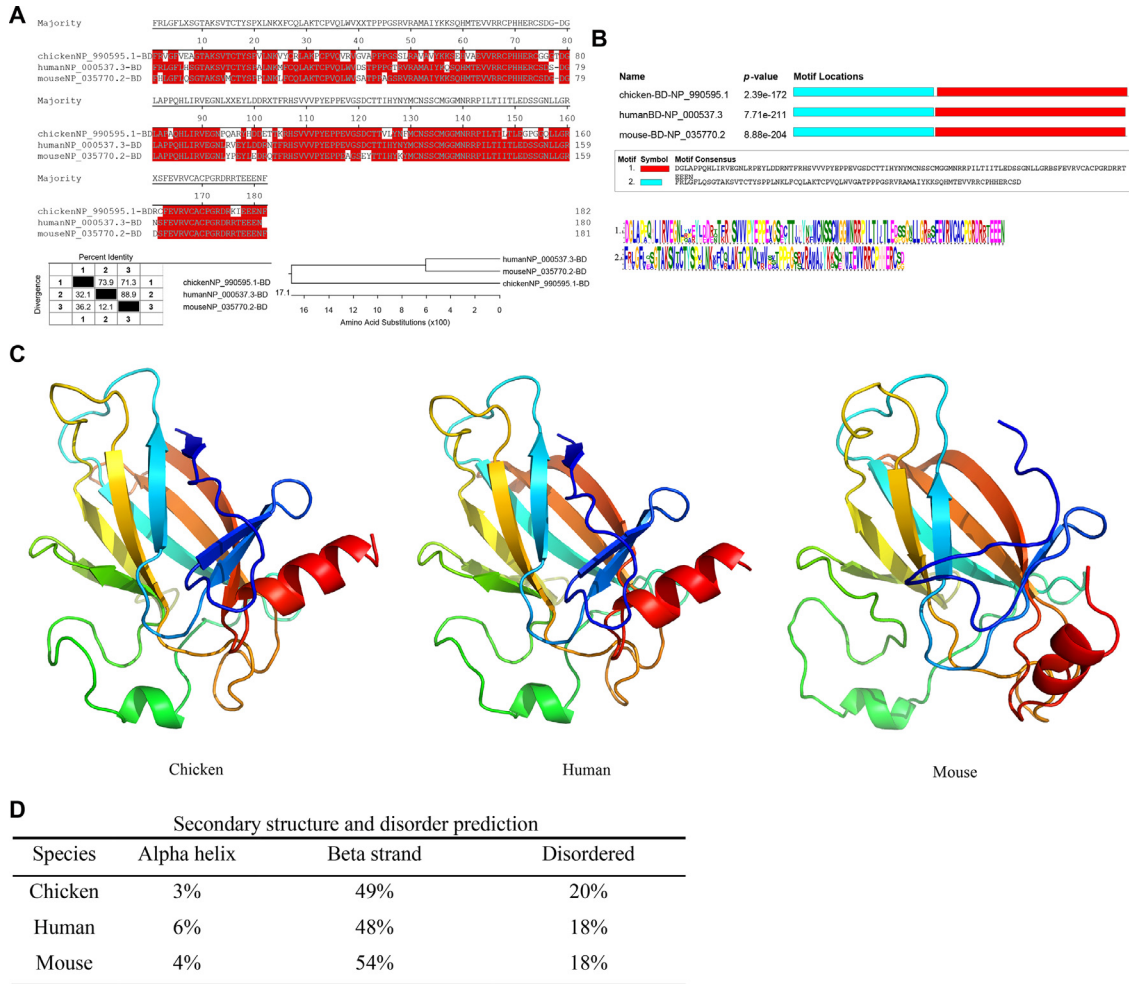


**Figure 7.** Comparative biological analysis of the predicted p53 DNA-binding domains. (A) The amino acid sequence analysis of p53 DNA-binding domains was performed using MegAlign 7.0.1, which included alignment reports, sequence distances, and phylogenetic trees. (B) The conserved motifs were determined using MEME with the p53 DNA-binding domain protein sequences. (C) In silico 3D prediction analyses for the three p53 DNA-binding domains were performed by the Phyre2 server. (D) Secondary structure and disorder prediction were also conducted by the Phyre2 server.

transcriptional regulation and provided data support for further research in this field.

Our cross-species analysis found that many classic p53-mediated biological processes were enriched by the direct target genes of both chicken p53 and human p53 (Figure 5D), indicating that the key functions of p53 may be conserved among species. However, the direct target genes and cofactors of regulation are quite different (Figures 5C and D), suggesting differences among species in the p53 target genes that perform the same function. The transactivation domain or transactivating domain (TAD) is a transcription factor scaffold domain that contains binding sites for other proteins such as transcription coregulators. These binding sites are frequently referred to as activation functions (AFs) (Anette et al., 2003). The absence of the TAD domain in chicken p53 compared to human and mouse p53 (Figure 6C) may partially explain the difference in genes targeted to p53 among species. In addition, among the 2.5% of the human sequences aligned with chickens (International Chicken Genome Sequencing Consortium, 2004), 44% are located in protein-coding regions, 25% are intronic, and 31% are intergenic, indicating

that promoter/genic regions tend to be more conserved than intronic and intergenic regions. Our analysis of the locations of chp53 genomic binding sites revealed that 39.89% are located in promoter regions, 28.19% are intronic, and 23.51% are intergenic (Figure 2A), which are generally identical to the proportions of these regions in human-chicken conserved sequences. Thus, our data indicate that chp53 genomic binding sites tend to occur in conserved regions. However, the core cofactors and the targeted motif of chp53 are similar to those of humans (Figure 4E and Figure 5C). This is because, despite the great differences in the full amino acid sequences of p53 among chickens, humans, and mice (Figure 6), both the amino acid sequences and the simulated three-dimensional structures of the DNA binding domain of p53 are highly conserved (Figure 7). Therefore, from the perspective of comparative biology, the sequences and structures of functional domains, the sequences of p53 target sites on the genome, and at least part of its key biological functions are relatively conserved across species.

In the present study, genome-wide transcriptional regulation by chicken p53 was conducted using the chicken

hepatoma cell line, LMH, which is a permissive cell line for ILTV infection and has been used in vitro to study the viral-host interactions of ILTV in our previous studies. In this model, we discovered an important regulatory role of *chp53* in ILTV replication by p53 activation and inhibition (Li et al., 2016; Li et al., 2018; Wang et al., 2019; Qiao et al., 2020; Wang et al., 2021; Xu et al., 2022). In the chicken fibroblast cell line, DF-1, which is nonpermissive for ILTV, remarkable activation of *chp53* upon IBDV infection was reported, and overexpression of *chp53* inhibited IBDV replication and upregulated the expressions of multiple chicken antiviral innate immunity genes (e.g., *IPS-1*, *IRF3*, *PKR*, *OAS*, and *MX*), whereas suppression of *chp53* led to the opposite effect (Ouyang et al., 2017). Our present study provides a comprehensive view of the antiviral functions of *chp53*. While, as the cell line we used here, the ChIP-seq experiments for human p53 were mainly applied in cancer cells too (Koeppel et al., 2011; Nikulenkov et al., 2012; Hafner et al., 2017). Given the high tumor-suppressor potency of p53 and the induction of cell death of LMH cells by ectopically expressing p53 that we observed (Figure 1D), our data may also contribute to the exploration of *chp53* targets and networks related to responding to the cancerogenesis in chickens.

In conclusion, our study identified 754 chicken p53 target genes and conducted a preliminary comparative biological analysis with humans and mice. These results are expected to help harness p53 activity by targeting p53 modulators and achieve a desired p53 transcriptional response in chickens in the future.

## ACKNOWLEDGMENTS

We are grateful to Yulong Gao (Harbin Veterinary Research Institute, Harbin, China), Zhiyong Ma (Shanghai Veterinary Research Institute, Shanghai, China), Yafeng Qiu (Shanghai Veterinary Research Institute, Shanghai, China), and other colleagues for providing experimental materials, technical support, and valuable suggestions.

This work was supported by the National Natural Science Foundation of China [grant number 32072853], the Natural Science Foundation of Heilongjiang Province of China [grant number JQ2021C006], and the Agriculture Research System of China [grant number CARS-40-K18].

## DISCLOSURES

The authors declare that there is no conflict of interest.

## SUPPLEMENTARY MATERIALS

Supplementary material associated with this article can be found, in the online version, at [doi:10.1016/j.psj.2022.102164](https://doi.org/10.1016/j.psj.2022.102164).

## REFERENCES

- Albina, J. E., S. Cui, R. B. Mateo, and J. S. Reichner. 1993. Nitric oxide-mediated apoptosis in murine peritoneal macrophages. *J. Immunol.* 150:5080–5085.
- Anette, W., T. Eckardt, A. P. H. Wright, and G. Jan-Ake. 2003. Activation functions 1 and 2 of nuclear receptors: molecular strategies for transcriptional activation. *Mol. Endocrinol.* 17:1901–1909.
- Bailey, T. L., J. Johnson, C. E. Grant, and W. S. Noble. 2015. The MEME suite. *Nucleic. Acids Res.* 43(W1):W39–W49.
- Biegging, K. T., and L. D. Attardi. 2012. Deconstructing p53 transcriptional networks in tumor suppression. *Trends. Cell Biol.* 22:97–106.
- Blankenberg, D., G. Von Kuster, N. Coraor, G. Ananda, R. Lazarus, M. Mangan, A. Nekrutenko, and J. Taylor. 2010. Galaxy: a web-based genome analysis tool for experimentalists. *Curr. Protoc. Mol. Biol.* 10:11–21 Chapter 19, Unit 19.
- Chen, C., H. Chen, Y. Zhang, H. R. Thomas, M. H. Frank, Y. He, and R. Xia. 2020. Tbttools: an integrative toolkit developed for interactive analyses of big biological data. *Mol. Plant.* 13:1194–1202.
- Deng, X., X. Li, Y. Shen, Y. Qiu, Z. Shi, D. Shao, Y. Jin, H. Chen, C. Ding, L. Li, P. Chen, and Z. Ma. 2010. The Meq oncoprotein of Marek's disease virus interacts with p53 and inhibits its transcriptional and apoptotic activities. *Virology.* 40:1–11.
- Dharel, N., N. Kato, R. Muroyama, H. Taniguchi, M. Otsuka, Y. Wang, A. Jazag, R. X. Shao, J. H. Chang, M. K. Adler, T. Kawabe, and M. Omata. 2008. Potential contribution of tumor suppressor p53 in the host defense against hepatitis C virus. *Hepatology.* 47:1136–1149.
- Garijo, R., P. Hernandez-Alonso, C. Rivas, J. S. Diallo, and R. Sanjuan. 2014. Experimental evolution of an oncolytic vesicular stomatitis virus with increased selectivity for p53-deficient cells. *Plos One.* 9:e102365.
- Hafner, A., J. Stewart-Ornstein, J. E. Purvis, W. C. Forrester, M. L. Bulyk, and G. Lahav. 2017. p53 pulses lead to distinct patterns of gene expression albeit similar DNA-binding dynamics. *Nat. Struct. Mol. Biol.* 24:840–847.
- Harris, S. L., and A. J. Levine. 2005. The p53 pathway: positive and negative feedback loops. *Oncogene.* 24:2899–2908.
- Ho Sui, S. J., J. R. Mortimer, D. J. Arenillas, J. Brumm, C. J. Walsh, B. P. Kennedy, and W. W. Wasserman. 2005. oPOSSUM: identification of over-represented transcription factor binding sites in co-expressed genes. *Nucleic. Acids Res.* 33:3154–3164.
- Hsu, T. H., C. C. Chu, S. Y. Jiang, M. W. Hung, W. C. Ni, H. E. Lin, and T. C. Chang. 2012. Expression of the class II tumor suppressor gene RIG1 is directly regulated by p53 tumor suppressor in cancer cell lines. *Febs. Lett.* 586:1287–1293.
- Huang, D. W., B. T. Sherman, and R. A. Lempicki. 2009. Systematic and integrative analysis of large gene lists using DAVID bioinformatics resources. *Nat. Protoc.* 4:44–57.
- Huang, Q. C., L. Zhan, H. Y. Cao, J. B. Li, Y. H. Lyu, X. Guo, J. Zhang, L. L. Ji, T. T. Ren, J. Z. An, B. R. Liu, Y. Z. Nie, and J. L. Xing. 2016. Increased mitochondrial fission promotes autophagy and hepatocellular carcinoma cell survival through the ROS-modulated coordinated regulation of the NFkB and TP53 pathways. *Autophagy.* 12:999–1014.
- International Chicken Genome Sequencing Consortium. 2004. Sequence and comparative analysis of the chicken genome provide unique perspectives on vertebrate evolution. *Nature.* 432:695–716.
- Jiang, D., E. L. LaGory, D. K. Broz, K. T. Biegging, C. A. Brady, N. Link, J. M. Abrams, A. J. Giaccia, and L. D. Attardi. 2015. Analysis of p53 transactivation domain mutants reveals Acad11 as a metabolic target important for p53 pro-survival function. *Cell Rep.* 10:1096–1109.
- Kelley, L. A., S. Mezulis, C. M. Yates, M. N. Wass, and M. J. E. Sternberg. 2015. The Phyre2 web portal for protein modeling, prediction and analysis. *Nat. Protoc.* 10:845–858.
- Koeppel, M., S. J. van Heeringen, D. Kramer, L. Smeenk, E. Janssen-Megens, M. Hartmann, H. G. Stunnenberg, and M. Lohrum. 2011. Crosstalk between c-Jun and TAp73alpha/beta contributes to the apoptosis-survival balance. *Nucleic. Acids Res.* 39:6069–6085.
- Lawrence, M. S., P. Stojanov, C. H. Mermel, J. T. Robinson, L. A. Garraway, T. R. Golub, M. Meyerson, S. B. Gabriel, E. S. Lander, and G. Getz. 2014. Discovery and saturation analysis of cancer genes across 21 tumour types. *Nature.* 505:495–501.
- Levine, A. J., and M. Oren. 2009. The first 30 years of p53: growing ever more complex. *Nat. Rev. Cancer.* 9:749–758.

- Li, H., Q. Gao, Y. H. Shao, B. Y. Sun, F. J. Wang, Y. Y. Qiao, N. N. Wang, and S. W. Liu. 2018. Gallid Herpesvirus 1 initiates apoptosis in uninfected cells through paracrine repression of p53. *J. Virol.* 92:e00529-18.
- Li, H., T. Lakshminanth, C. Garofalo, M. Enge, C. Spinnler, A. Anichini, L. Szekely, K. Karre, E. Carbone, and G. Selivanova. 2011. Pharmacological activation of p53 triggers anticancer innate immune response through induction of ULBP2. *Cell Cycle.* 10:3346–3358.
- Li, H., F. J. Wang, Z. X. Han, Q. Gao, H. X. Li, Y. H. Shao, N. N. Sun, and S. W. Liu. 2016. Genome-wide gene expression analysis identifies the proto-oncogene tyrosine-protein kinase SRC as a crucial virulence determinant of infectious laryngotracheitis virus in chicken cells. *J. Virol.* 90:9–21.
- Li, H., Y. Zhang, A. Strose, D. Tedesco, K. Gurova, and G. Selivanova. 2014. Integrated high-throughput analysis identifies Sp1 as a crucial determinant of p53-mediated apoptosis. *Cell Death Differ.* 21:1493–1502.
- Li, M., Y. He, W. Dubois, X. Wu, J. Shi, and J. Huang. 2012. Distinct regulatory mechanisms and functions for p53-activated and p53-repressed DNA damage response genes in embryonic stem cells. *Mol. Cell.* 46:30–42.
- Liu, W. L., X. X. Li, E. S. H. Chu, M. Y. Y. Go, L. X. Xu, G. J. Zhao, L. L. Li, N. Dai, J. M. Si, Q. A. Tao, J. J. Y. Sung, and L. Yu. 2011. Paired box gene 5 is a novel tumor suppressor in hepatocellular carcinoma through interaction with p53 signaling pathway. *Hepatology.* 53:843–853.
- Lujambio, A., L. Akkari, J. Simon, D. Grace, D. F. Tschaharganeh, J. E. Bolden, Z. Zhao, V. Thapar, J. A. Joyce, V. Krizhanovsky, and S. W. Lowe. 2013. Non-cell-autonomous tumor suppression by p53. *Cell.* 153:449–460.
- Menendez, D., A. Inga, and M. A. Resnick. 2009. The expanding universe of p53 targets. *Nat. Rev. Cancer.* 9:724–737.
- Messmer, U. K., and B. Brune. 1996. Nitric oxide-induced apoptosis: p53-dependent and p53-independent signalling pathways. *Biochem. J.* 319:299–305.
- Munoz-Fontela, C., M. A. Garcia, I. Garcia-Cao, M. Collado, J. Arroyo, M. Esteban, M. Serrano, and C. Rivas. 2005. Resistance to viral infection of super p53 mice. *Oncogene.* 24:3059–3062.
- Nikulenkov, F., C. Spinnler, H. Li, C. Tonelli, Y. Shi, M. Turunen, T. Kivioja, I. Ignatiev, A. Kel, J. Taipale, and G. Selivanova. 2012. Insights into p53 transcriptional function via genome-wide chromatin occupancy and gene expression analysis. *Cell Death Differ.* 19:1992–2002.
- Ouyang, W., Y. S. Wang, K. Meng, Q. X. Pan, X. L. Wang, X. X. Xia, Y. M. Zhu, Z. W. Bi, H. B. Zhang, and K. Luo. 2017. gga-miR-2127 downregulates the translation of chicken p53 and attenuates chp53-mediated innate immune response against IBVD infection. *Vet. Microbiol.* 198:34–42.
- Pampin, M., Y. Simonin, B. Blondel, Y. Percherancier, and M. K. Chelbi-Alix. 2006. Cross talk between PML and p53 during poliovirus infection: implications for antiviral defense. *J. Virol.* 80:8582–8592.
- Qiao, Y. Y., Z. T. Wang, Z. X. Han, Y. H. Shao, Y. Ma, Y. M. Liang, Z. J. Chen, H. G. Wu, L. Cui, Y. H. Zhang, S. W. Liu, and H. Li. 2020. Global exploration of the metabolic requirements of Gallid Alpha herpesvirus 1. *PLoS Pathog.* 16:e1008815.
- Riley, T., E. Sontag, P. Chen, and A. Levine. 2008. Transcriptional control of human p53-regulated genes. *Nat. Rev. Mol. Cell Biol.* 9:402–412.
- Schwitalla, S., P. K. Ziegler, D. Horst, V. Becker, I. Kerle, Y. Begus-Nahrmann, A. Lechel, K. L. Rudolph, R. Langer, J. Slotta-Huspenina, F. G. Bader, O. Prazeres da Costa, M. F. Neurath, A. Meining, T. Kirchner, and F. R. Greten. 2013. Loss of p53 in enterocytes generates an inflammatory microenvironment enabling invasion and lymph node metastasis of carcinoma-induced colorectal tumors. *Cancer Cell.* 23:93–106.
- Shannon, P., A. Markiel, O. Ozier, N. S. Baliga, J. T. Wang, D. Ramage, N. Amin, B. Schwikowski, and T. Ideker. 2003. Cytoscape: a software environment for integrated models of biomolecular interaction networks. *Genome Res.* 13:2498–2504.
- Shatz, M., D. Menendez, and M. A. Resnick. 2012. The human TLR innate immune gene family is differentially influenced by DNA stress and p53 status in cancer cells. *Cancer Res.* 72:3948–3957.
- Smeenk, L., S. J. van Heeringen, M. Koepfel, M. A. van Driel, S. J. J. Bartels, R. C. Akkers, S. Denissov, H. G. Stunnenberg, and M. Lohrum. 2008. Characterization of genome-wide p53-binding sites upon stress response. *Nucleic. Acids Res.* 36:3639–3654.
- Szklarczyk, D., A. L. Gable, D. Lyon, A. Junge, S. Wyder, J. Huerta-Cepas, M. Simonovic, N. T. Doncheva, J. H. Morris, P. Bork, L. J. Jensen, and C. Mering. 2019. STRING v11: protein-protein association networks with increased coverage, supporting functional discovery in genome-wide experimental datasets. *Nucleic. Acids Res.* 47(D1):D607–D613.
- Taura, M., A. Eguma, M. A. Suico, T. Shuto, T. Koga, K. Komatsu, T. Komune, T. Sato, H. Saya, J. D. Li, and H. Kai. 2008. p53 regulates toll-like receptor 3 expression and function in human epithelial cell lines. *Mol. Cell Biol.* 28:6557–6567.
- Textor, S., N. Fiegler, A. Arnold, A. Porgador, T. G. Hofmann, and A. Cerwenka. 2011. Human NK cells are alerted to induction of p53 in cancer cells by upregulation of the NKG2D ligands ULBP1 and ULBP2. *Cancer Res.* 71:5998–6009.
- Thiery, J., S. Abouzahr, G. Dorothee, A. Jalil, C. Richon, I. Vergnon, F. Mami-Chouaib, and S. Chouaib. 2005. p53 potentiation of tumor cell susceptibility to CTL involves Fas and mitochondrial pathways. *J. Immunol.* 174:871–878.
- Tonelli, C., M. J. Morelli, A. Sabò, A. Verrecchia, L. Rotta, T. Capra, S. Bianchi, S. Campaner, and B. Amati. 2017. Genome-wide analysis of p53-regulated transcription in Myc-driven lymphomas. *Oncogene.* 36:2921–2929.
- Vogelstein, B., D. Lane, and A. J. Levine. 2000. Surfing the p53 network. *Nature.* 408:307–310.
- Wang, B., D. Niu, L. Lai, and E. C. Ren. 2013. p53 increases MHC class I expression by upregulating the endoplasmic reticulum aminopeptidase ERAP1. *Nat. Commun.* 4:2359.
- Wang, Z. T., Y. Y. Qiao, Z. J. Chen, Y. M. Liang, L. Cui, Y. H. Zhang, X. F. Li, L. Xu, P. Wei, S. W. Liu, and H. Li. 2021. Fos facilitates Gallid Alpha-Herpesvirus 1 infection by transcriptional control of host metabolic genes and viral immediate early gene. *Viruses.* 13:1110.
- Wang, Z. T., B. Y. Sun, Q. Gao, Y. Ma, Y. M. Liang, Z. J. Chen, H. G. Wu, L. Cui, Y. H. Shao, P. Wei, H. Li, and S. W. Liu. 2019. Host Src controls Gallid Alpha Herpesvirus 1 intercellular spread in a cellular fatty acid metabolism-dependent manner. *Virology.* 537:1–13.
- Wei, C. L., Q. Wu, V. B. Vega, K. P. Chiu, P. Ng, T. Zhang, A. Shahab, H. C. Yong, Y. T. Fu, Z. P. Weng, J. J. Liu, X. D. Zhao, J. L. Chew, Y. L. Lee, V. A. Kuznetsov, W. K. Sung, L. D. Miller, B. Lim, E. T. Liu, Q. Yu, H. H. Ng, and Y. J. Ruan. 2006. A global map of p53 transcription-factor binding sites in the human genome. *Cell.* 124:207–219.
- Xu, L., Z. Wang, Z. Chen, L. Cui, Z. Liu, Y. Liang, X. Li, Y. Zhang, S. Liu, and H. Li. 2022. PFT- $\alpha$  inhibits gallid alpha herpesvirus 1 replication by repressing host nucleotide metabolism and ATP synthesis. *Vet. Microbiol.* 269:109435.
- Xue, W., L. Zender, C. Miething, R. A. Dickins, E. Hernando, V. Krizhanovsky, C. Cordon-Cardo, and S. W. Lowe. 2007. Senescence and tumour clearance is triggered by p53 restoration in murine liver carcinomas. *Nature.* 445:656–660.
- Yan, W. J., J. C. Wei, X. F. Deng, Z. X. Shi, Z. X. Zhu, D. H. Shao, B. B. Li, S. H. Wang, G. Z. Tong, and Z. Y. Ma. 2015. Transcriptional analysis of immune-related gene expression in p53-deficient mice with increased susceptibility to influenza A virus infection. *BMC Med. Genomics.* 8:52.
- Yu, G., L. G. Wang, and Q. Y. He. 2015. ChIPseeker: an R/Bioconductor package for ChIP peak annotation, comparison and visualization. *Bioinformatics* 31:2382–2383.
- Zhang, H., H. Zhang, S. Cao, C. Sui, Y. Song, Y. Zhao, and S. Liu. 2021. Knockout of p53 leads to a significant increase in ALV-J replication. *Poult. Sci.* 100:101374.
- Zhang, Y., C. Y. Zhu, B. Y. Sun, J. W. Lv, Z. H. Liu, S. W. Liu, and H. Li. 2017. Integrated high throughput analysis identifies GSK3 as a crucial determinant of p53-mediated apoptosis in lung cancer cells. *Cell Physiol. Biochem.* 42:1177–1191.
- Zhu, K., J. Wang, J. Zhu, J. Jiang, J. Shou, and X. Chen. 1999. p53 induces TAP1 and enhances the transport of MHC class I peptides. *Oncogene* 18:7740–7747.
- Zhu, Z., Y. Yang, J. Wei, D. Shao, Z. Shi, B. Li, K. Liu, Y. Qiu, H. Zheng, and Z. Ma. 2014. Type I interferon-mediated immune response against influenza A virus is attenuated in the absence of p53. *Biochem. Biophys. Res. Commun.* 454:189–195.
- Zwang, Y., M. Oren, and Y. Yarden. 2012. Consistency test of the cell cycle: roles for p53 and EGR1. *Cancer Res.* 72:1051–1054.